Applied Catalysis B: Environmental 320 (2023) 121959

Contents lists available at ScienceDirect

Applied Catalysis B: Environmental

journal homepage: www.elsevier.com/locate/apcatb

Identifying limitations in screening high-throughput photocatalytic bimetallic nanoparticles with machine-learned hydrogen adsorptions

Kirby Broderick [a], Eric Lopato [b], Brook Wander [a], Stefan Bernhard [b], John Kitchin [a], Zachary Ulissi [a,*]

[a] Department of Chemical Engineering, Carnegie Mellon University, 5000 Forbes Avenue, Pittsburgh, PA 15213, USA
[b] Department of Chemistry, Carnegie Mellon University, 4400 Fifth Avenue, Pittsburgh, PA 15213, USA

ARTICLE INFO

Keywords:
Hydrogen Evolution Reaction
Computational catalysis
Sabatier principle
High-throughput screening
Nanocatalysis

ABSTRACT

The Sabatier principle is of fundamental importance to computational catalyst discovery, saving researchers time and expense by predicting catalytic activity in silico at scale. However, as polycrystalline and nanoscale catalysts increasingly dominate industry, computational screening tools must be adapted to these uses. In this work, we demonstrate the effectiveness of computational adsorption energy screening in nanocatalysis by comparing a multisite adsorption energy prediction workflow against a large experimental dataset of hydrogen evolution activities over bimetallic nanoparticles. Comparing 16 million hydrogen adsorption energy predictions with the hydrogen evolution activity of 5300 experiments across 84 monometallic and bimetallic systems, we discover that favorable adsorption energies are a necessary condition for experimental activity, but other factors often determine trends in practice. About half of the bimetallic search space can be excluded from experimental screens using hydrogen adsorption predictions, but this method may become significantly more powerful when combined with other screening tools.

1. Introduction

The discovery of new catalysts for fundamental reactions such as water splitting, ammonia synthesis, or CO_2 reduction is a fundamental to the development of an environmentally sustainable economy. By increasing reaction efficiency, catalysts offer the possibility of reducing industrial energy requirements and enabling more sustainable chemical production processes [1]. However, the space of all possible catalysts is too vast to be surveyed experimentally [2]. For this reason, the field of computational catalysis tries to predict catalytic activity using materials properties. One important tool is the Sabatier principle, which describes a volcano-shaped relationship between the binding energy of a key reaction specie and the overall reaction rate [3]. Although this relationship was developed using experimental binding energies [4], these values can be computed using Density Functional Theory (DFT), a computationally tractable approximation to quantum chemistry [1,5].

Modern efforts to computationally screen chemical composition space for new catalysts began almost two decades ago. Nørskov et al. [6] established a kinetic model that uses DFT-calculated ΔE(*H) on an fcc site to predict exchange current density. This work also considered the effects of changing coverage and found them to be minimal. Later efforts by the same group looked at multiple adsorption sites in more detail, screening bimetallic alloys modeled as a pure metal with a secondary metal incorporated into the surface layer [7] and further developing the kinetic model [8] (see Fig. 1). The latter work used 1 monolayer coverage for all materials on the left half of the volcano. The researchers also made the observation that, despite the fact that many of the metals on the left-hand side of the volcano should be oxidized, experimental values align with adsorption calculations made using metallic surfaces.

The development of computationally grounded volcano plots has spurred researchers to find ways to optimize and streamline their use in catalytic discovery. Tran and Ulissi [2] established a high-throughput automated screening method using active learning to discover materials with binding energies that indicate activity for hydrogen evolution and CO_2 reduction. Another effort established a data set of DFT calculations and associated community challenges to spur interest in machine learning models capable of approximating DFT adsorption energies across a variety of adsorbates and materials for catalyst discovery [10].

However, several complications differentiate industrial catalysts from the slab models commonly used to compute adsorption energies [2,

* Corresponding author.
E-mail address: zulissi@andrew.cmu.edu (Z. Ulissi).

https://doi.org/10.1016/j.apcatb.2022.121959
Received 23 June 2022; Received in revised form 30 August 2022; Accepted 5 September 2022
Available online 21 September 2022

6]. Modern industrial catalysts are often highly nanostructured, experiencing size-specific chemical phenomena that impact catalysis [11], and nanoparticles may undergo surface or bulk segregation to form a distribution of structures and surfaces in practice [12,13]. Furthermore, it is not always clear which surfaces and binding sites are most responsible for catalytic activity, which is confounded by the difficulty of experimentally characterizing structure or surface expression at the scale of modern computational and experimental screens [14]. Bimetallic nanoparticles have been of interest for their catalytic properties for many reactions in recent decades [15,16]. The expanded bimetallic material search space offers the possibility of discovering cheaper or more active catalysts while remaining tractable using modern computational techniques [2].

There is also uncertainty regarding the effects of modifications to the chemical environment on the computational Sabatier relationship. The hydrogen atom is extremely small and typically binds closely to the surface, so its adsorption energy is likely to be minimally affected by the solvation environment, and work establishing DFT-based volcano plots found that water and an additional electrostatic field had a minimal effect on hydrogen adsorption energies [17]. However, the physical reaction will be modified by the solvation environment, and a variety of strategies have been proposed to account for different solvation effects. The Hydrogen Evolution Reaction (HER) proceeds slower in alkaline solutions than acidic ones, owing to the different proton donor. Zheng et al. formulated an "apparent hydrogen binding energy" H_{app} that accounts for the effects of pH on the desorption of water corresponding to a hydrogen adsorption event in a solvated environment, although this requires cyclic voltammetry data that cannot be easily obtained at scale [18]. It is in principle possible to account for the solvent reorganization energy associated with electron transfer as in Marcus theory, although this is difficult in practice [19]. A discussion of the effects of organic electrolytes can be found in [20]. In our case, the fact that the solvent, DMSO, is not a proton donor and forms hydrogen bonds with water will reduce proton activity (as described in [21,22]), but no tools exist to our knowledge that can readily be adapted to the scale of experiments or computation used in this work. Additionally, because our workflow precipitates metal ions in situ, there will be metal ions in solution at some low concentration during experiments, and further precipitation will compete with hydrogen evolution for available reductant. However, the total amount of metal ions available in solution is small enough relative to the number of protons that we believe this effect is negligible.

In previous work, we developed a high-throughput method for synthesizing bimetallic nanoparticles and measuring their ability to catalyze the HER [23–25]. In this procedure, metal salts are combined with a photocatalyst, and light stimulates the reduction of ions into nanoparticles and the subsequent evolution of hydrogen gas (see Fig. 2). By holding the intensity of light and concentration and identity of the photocatalyst constant, we limit the effects of variation in the electron delivery pathway on differential catalytic activity across experiments, although variations in catalytic activity have been observed based on the

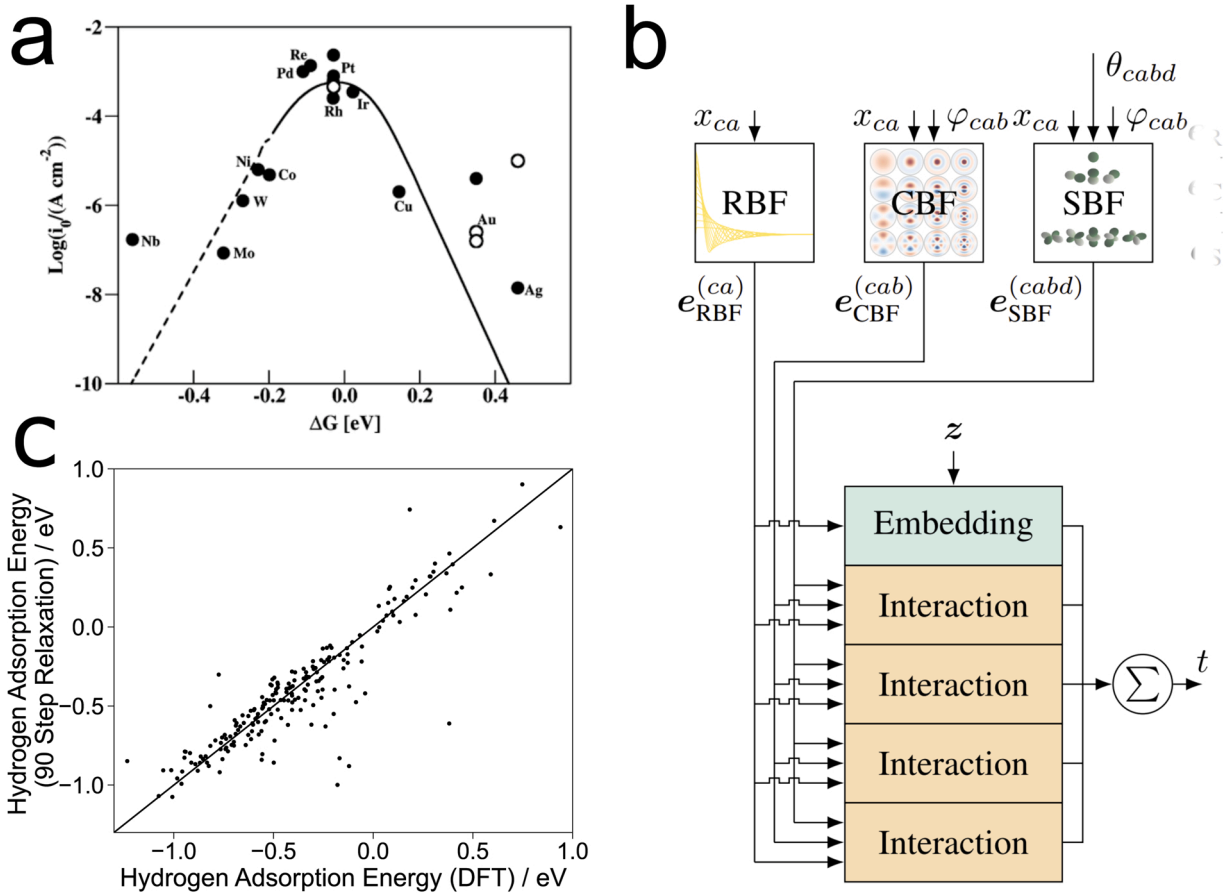

Fig. 1. (a) A volcano plot for hydrogen evolution taken from Skúlason et al. [8]. Measured exchange current density is plotted against the free energy of hydrogen adsorption at U = 0 V. Adsorption energies were calculated using DFT, assuming 0.25 monolayer coverage for metals on the right-hand side of the volcano, and 1 monolayer coverage otherwise. The kinetic model is represented as a line; the dashed line represents the expectation that metals this strong binding will oxidize. (b) A block diagram detailing the structure of GemNet, the message-passing graph neural network used in this work to model DFT hydrogen adsorption energies, taken from Klicpera et al. [9]. These adsorption energies are used to construct the x-axis of the volcano plot used in this work. (c) A parity plot comparing the predicted hydrogen adsorption energy after a 90-step relaxation using the model depicted in (b) to DFT validation data. This demonstrates the accuracy of the machine learned model (MAE = 0.1 eV).

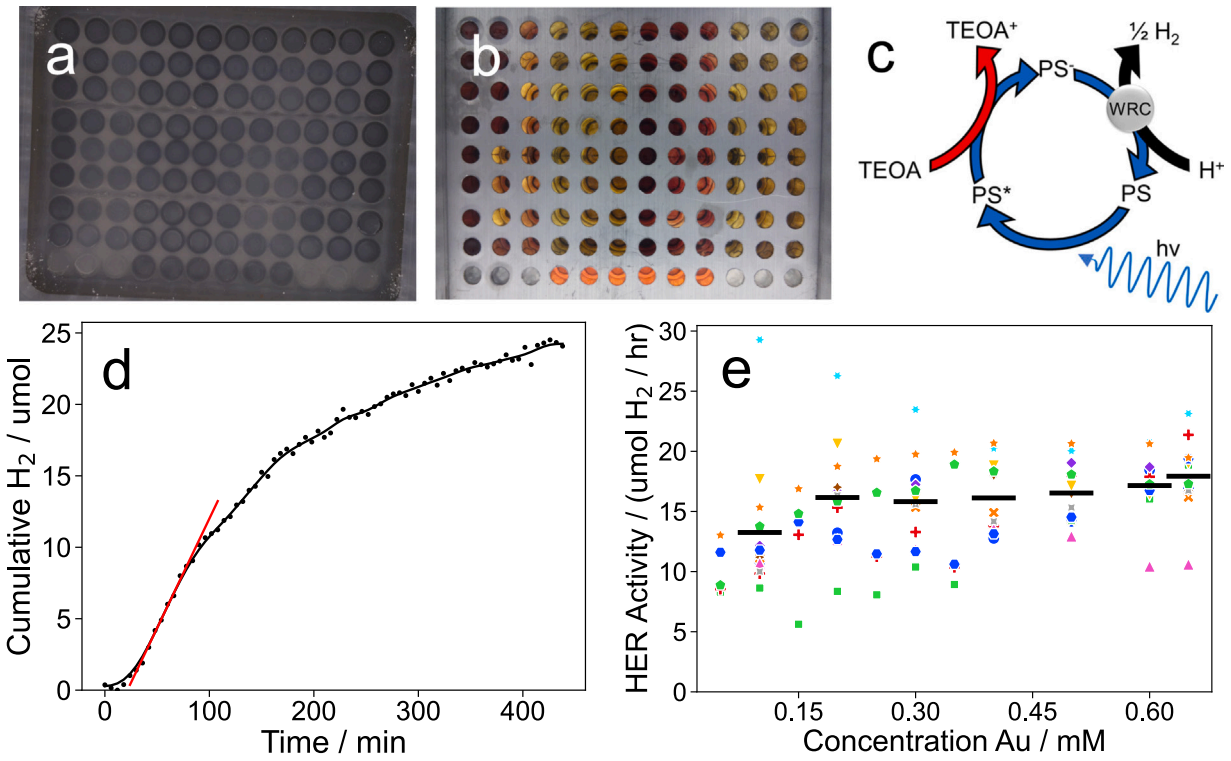

Fig. 2. (a) An image of an experimental well plate during a hydrogen evolution experiment. Darkening of the wells over time corresponds to hydrogen adsorption onto a chemosensory tape, which is then used to determine cumulative hydrogen evolution. (b) The underside of a well plate during an experiment. (c) The proposed catalytic cycle for hydrogen evolution observed in experiments in this work [23]. The photosensitizer is charged by a sacrificial oxidant and then reduces a catalyst, resulting in the formation of hydrogen from water. The only component of this pathway that changes across experiments is the catalyst ("WRC"), which is not generally photoactive. (d) Time series data for the cumulative evolution of hydrogen over time for a single well in an experiment. The slope of the red line denotes the maximum rate observed. This maximum rate is aggregated across multiple experiments with the same metal combination and the resulting value is used in place of exchange current density as the y-axis of our volcano plot. (e) The observed maximum HER rates for various experiments containing only Au metal salt. Rates from experiments that ran concurrently in different wells are plotted using the same color and shape. Rates were averaged across all experiments that used the same metal salts at the same concentrations (average values are depicted as black bars), and the highest average rate is used to represent the metal system on the volcano plot.

choice of electron delivery pathway [26]. In this work, we assess the sufficiency of hydrogen adsorption energy predictions in describing the resulting data: the experimental HER activities of bimetallic nanoparticles are compared with a computational workflow that predicts and aggregates hydrogen adsorption energies across various surfaces from intermetallic crystal structures from the Materials Project [27]. Although the Sabatier principle is not expected to be perfectly predictive due to factors we discuss in the Section 3, in this work, we assess its use as a screening tool across a large dataset of photocatalytic hydrogen evolution experiments. Our computational workflow is distinguished from previous efforts because it automates the process of predicting adsorption energies across different binding sites, surfaces, and materials, allowing catalysis experiment and theory to be compared at greater scales than previously possible.

2. Experimental

2.1. High-throughput synthesis and assay of bimetallic nanoparticles

To explore the expanse of bimetallic space for in situ nanoparticle synthesis, the concentration of two different precursor salts were varied in each column and row of a high-throughput photoreactor. Each vial comprised $[Ir(Fmppy)_2dtbbpy]PF_6$ photosensitizer at 0.25 mM concentration, 400 μL of DMSO (J.T. Baker JT9224), 40 μL of a 30% (w/w) aqueous TEOA (Alfa Aesar L04486) solution, and metal salts at concentrations varying between 0.05 and 0.65 μM. Experiments included the metals Ag, Al, Au, Bi, Co, Cr, Eu, Fe, Ga, In, Ir, La, Li, Mn, Mo, Ni, Os, Pb, Pd, Pt, Rh, Ru, Sn, V, and Zn. A list of metal salt precursors is given in the Supporting Information.

Reaction wells were illuminated over blue LEDs in a parallelized reactor setup as described previously. Using colorimetric chemosensitive H_2 detection tape (DetecTape Hydrogen Detection Tape-Midsun Specialty Products, Item DT-H210015-PF4), the reactions were tracked in real-time using image analysis to reveal the quantity of hydrogen produced by each. Calibrations for this method can be found in our previous work [23].

2.2. Computational enumeration and prediction of sites

Starting with the dataset of intermetallic Materials Project structures created from bulks with nonpositive formation energies at most 0.1 eV above hull enumerated in the Open Catalyst Dataset [10,27], slabs were enumerated using Open Catalyst Dataset enumeration tools, and CatKit was used to position adsorption sites over the surfaces [28]. All bare structures larger than 80 atoms and all slabs larger than 100 atoms were discarded due to computational constraints, representing less than 1 % of structures and approximately 30 % of slabs. Hydrogen adsorption energies of the adsorbate-slab systems were then calculated using GemNet, a graph neural network that uses message passing with directed edge embeddings to predict materials properties from structures [9]. The model had been trained on the Open Catalyst Dataset and is available on the Open Catalyst Project website [10]. Systems were relaxed using this model for 90 steps before energies were predicted, a procedure which accurately predicts validation data (see Fig. 1). After adsorption energies were predicted, the minimum (strongest) adsorption energy was taken to represent the surface.

2.3. Formation of volcano plot

For every metal system (e.g. Au-Ni), corresponding surface minimum adsorption energies were selected from the calculated adsorption energy data set based on whether the corresponding structure had a bulk electrochemical stability below 0.5 eV/atom as calculated using the Materials Project PourbaixDiagram module [29–31], assuming a pH of 8.5, a voltage of − 1.2 V [32], and every metal ion at a concentration of 0.6 mM (corresponding approximately to the upper end of experimental metal ion concentration). The minimum hydrogen binding energy on every facet was taken, then the value closest to − 0.24 eV (representing approximate thermodynamic neutrality after free energy correction [6]) was chosen to represent the overall binding energy of the chemical system. Experimental activities were calculated by smoothing observed cumulative hydrogen evolution over time with a Gaussian filter and taking the maximum rate for every trial (see Fig. 2). After averaging experimental values observed under identical input conditions, we used the maximum rate across every experiment within a metal system to represent chemical activity (see Fig. 3).

3. Results and discussion

3.1. Aggregating hydrogen binding energies across a chemical system

A single physical descriptor cannot capture the dynamics of such a complex process as in situ nanoparticle formation and catalysis, and uncertainty in the physical process makes it difficult to predict the outcome of individual trials directly without fine control of process conditions. Accurate and comprehensive models of nanoparticle formation, growth, or surface expression remain elusive, and current works typically use experimental characterization techniques to model small numbers of systems in detail [33–35], although some multisystem screening tools have been developed recently [36–38]. Experimental binding energies also often differ significantly from theoretical values, which are generally calculated using DFT over low-index intermetallic surfaces. Such complications include surface poisoning and passivation [39], transport limitations [40], and surface strain [11]. Of particular interest is coverage effects [41]. When the adsorption energy is low, the surface will be sparsely covered and the low-coverage site will be the most occupied, so the observed hydrogen adsorption energy will be close to the minimum binding site. For other surfaces, the adsorption energy of the active site may scale linearly with the adsorption energy of the low-coverage site. Although we do not account for coverage effects in this work, trends in the adsorption energy of the active site may match the low coverage trends even in materials that are partially or substantially covered in hydrogen [42]. The HER over a platinum surface, one of the fastest chemical reactions ever observed, appears to progress through a weak-binding adsorbed intermediate [43,44]. However, other sources argue that in spite of these factors, the Sabatier principle can be used as a heuristic to guide experimenters toward a subset of materials with the potential for activity [45,46].

With a view to this controversy, we observe that the most experimentally active chemical systems in our data contain materials with surfaces whose low-coverage binding energies are at or slightly stronger than thermodynamic neutrality (-0.41 eV $< \Delta E(H^*) < -0.23$ eV, see Fig. 4), whereas systems containing only thermodynamically unfavorable surfaces are less active, with the upper envelope of experimental activities relative to binding energies forming a volcano shape. This relationship is not perfect: a large number of chemical systems are predicted to express surfaces with favorable binding energies but are not very active experimentally. This observation is consistent with a physical picture in which aggregate reactivity is dominated by the most active surface present, but in some experiments this surface is deactivated or not present. One important caveat is that unlike in a Sabatier plot, plotted experimental activity is not normalized by surface area, meaning that data may underperform the Sabatier trend due to reduced surface area relative to the most active points. Additionally, this relationship is mediated by a substantial amount of noise in both the *x*- and *y*-axis (see Fig. 1, Fig. 2). The full set of predictions generated using this method for all metal combinations can be seen in Fig. 5.

3.2. Noble metals

Noble metals significantly outperformed base metals beyond what can be explained by adsorption thermodynamics alone (see Fig. 4). In the volcano-type plot developed in this work, the HER activity for all experiments involving at least one noble metal was on average about an order of magnitude higher than activities from experiments using only base metals even if both systems expressed surfaces of equivalent binding energies (see Fig. 4). One possible explanation of this trend is that, although base metals may express thermodynamically active surfaces, these surfaces are less experimentally common than active surfaces on noble metals, either because particles are less likely to form or surfaces are deactivated. The latter prediction is supported by the experimental observation of oxides and sulfides on iron and nickel particles in a similar experimental system [24]. Another compelling hypothesis is that 3d metals tend to have compact orbitals that cannot facilitate effective electron transfer [39]. However, the activity of weak-binding noble metals Au and Ag are also known to be significantly enhanced in nanoparticle form, with explanations for this trend including surface strain and surface cleanliness [47–51]. Alternatively, the active surfaces on noble metals may be less easily poisoned, aggregated, or passivated: these effects were not considered in this work. Differences in nanoparticle stability may also have a substantial effect on activity trends [25].

4. Conclusions

To address challenges in connecting simple descriptors with complicated experimental catalysts, we developed an approach grounded in the Sabatier principle that aggregates adsorption energies over many active sites on different surfaces across a chemical system. We evaluated the usefulness of this relationship by comparing hydrogen adsorption energies predicted by machine-learned DFT surrogate models to Hydrogen Evolution Reaction rates observed in a high-throughput experimental workflow outlined in previous work. In doing so, we discovered that thermodynamically favorable hydrogen adsorption sites are necessary for rapid hydrogen evolution but do not guarantee it, and we then outlined other factors, including poisoning, variation in nucleation and growth, surface expression, and strain effects, that may be modulating this relationship. This work extends the use of adsorption energy calculations as a useful catalyst screening tool to complex nanoparticle systems and increases demand for tools to understand other aspects of the catalytic process.

The model developed in this work extends catalyst design principles to large real-world datasets, representing an important step on the path to high-throughput in-the-loop materials discovery. Individual nanoparticle experiments can form materials with many compositions, structures, sizes, and surfaces that may show radically different catalyst activities, and we often cannot know beforehand what these distributions will look like. Materials discovery and design workflows need better strategies for modeling and learning these distributions automatically, which requires adapting and scaling well-known relationships as in this work. In particular, an understanding of the thermodynamic stability of materials and surfaces in different chemical environments will be important not only for understanding experimental observations but also in developing long-lasting catalysts for industrial use. Ultimately, as more advanced models are able to fit gaps in our current analytical understanding, they will ideally be integrated with experiments in closed-loop discovery workflows, accelerating and systematizing catalysis science.

The result in this work adds to a growing body of knowledge

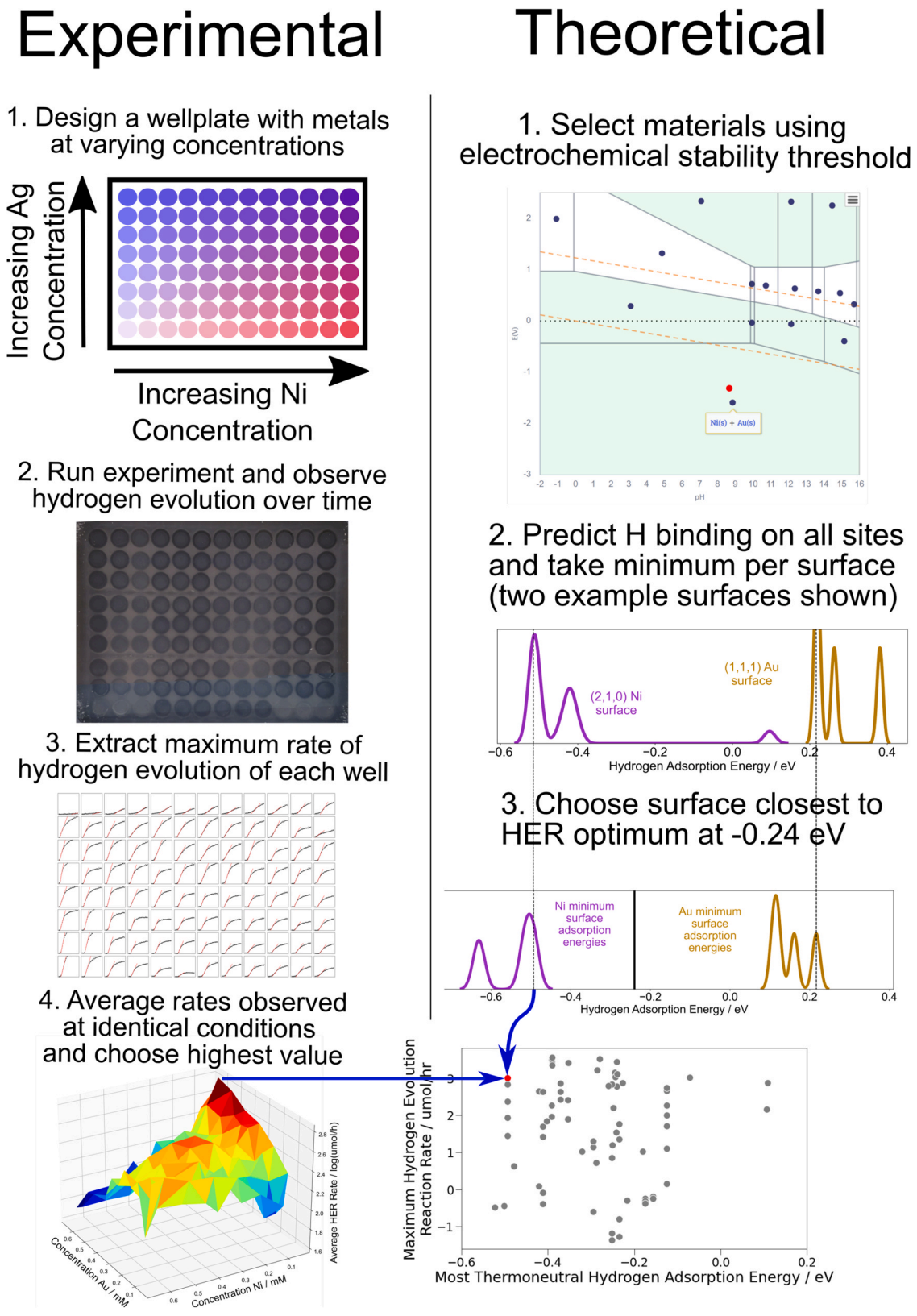

Fig. 3. A schematic detailing the formation of the volcano plot for the example of the gold-nickel system. (left) The y-axis of the volcano plot is constructed using a set of experiments conducted in the same chemical system (top left; a single well plate is shown). For each experiment, the maximum rate of change over time is determined after smoothing (center left), and then experiments conducted at the same conditions are averaged to create a map of maximum rate as a function of composition (bottom left). The highest value is then used to represent the reaction rate of the chemical system on the volcano plot (bottom right). (right) The x-axis of the volcano plot is constructed starting with crystal structures taken from the Materials Project. A Pourbaix Diagram is used to find stable crystals at representative chemical conditions (top right). Then, hydrogen adsorption energy predictions are made for enumerated sites, and the lowest value is taken for every surface on each crystal (two representative surfaces chosen). The surface closest to − 0.24 eV is used to represent the chemical system on the x-axis of the volcano plot (bottom right).

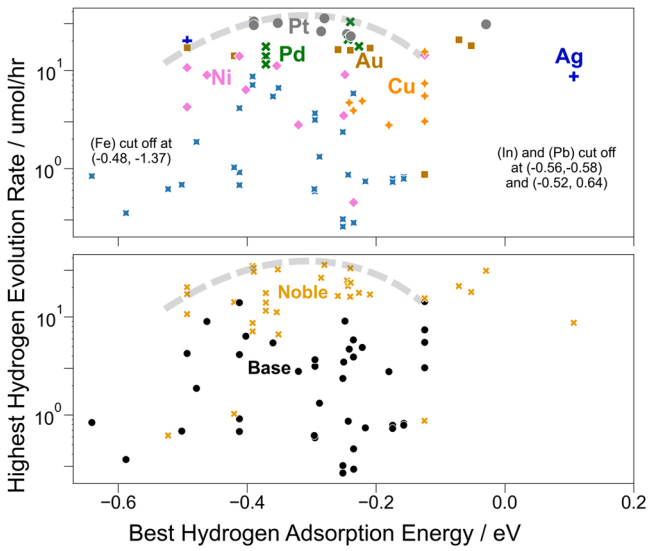

Fig. 4. Volcano plots constructed by plotting the surface low-coverage hydrogen adsorption energy closest to the optimum (i.e. the surface minimum hydrogen adsorption energy closest to − 0.24 eV) across all stable materials in for each metal combination against the highest experimental HER rate observed over all metal salt concentrations for that combination. A grey trend is drawn on as a guide for the eye. The four points to the right that lie above the trend contain Au and Ag, which are known to have improved hydrogen adsorption energies in nanoparticle form due to surface strain [47,48]; the adsorption energies used in this work do not account for that effect. Note that the y-axis is not normalized by surface area, meaning that differences in absolute rates are affected by variations in the area of the total reactive interface. Materials with binding energies above 0.2 (pure In and Pb) were removed for clarity; neither was experimentally active in any solvent condition. (a) This plot is colored by the metal in each bimetallic composition that had the highest pure activity: Pt (grey), Au (orange), Pd (green), Ni (pink), or Cu (orange). (b) This plot is colored by the presence (gold) or absence (black) of a noble metal. Across all solvent conditions, experiments containing at least one noble metal (shown in gold) tend to fall above the rest (black) at similar points on the x-axis.

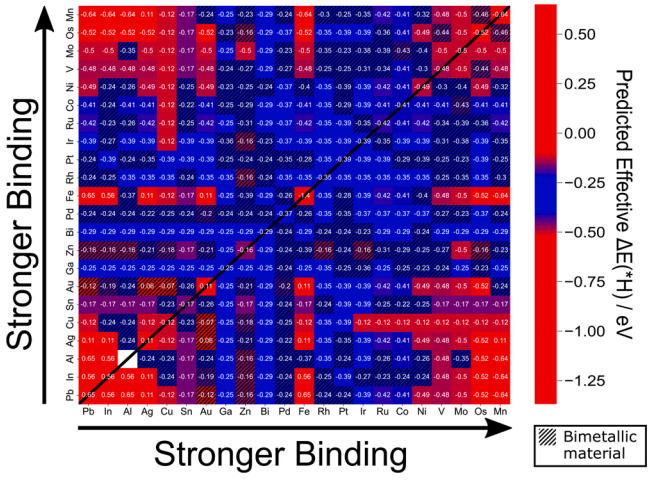

Fig. 5. A grid plot of the predicted hydrogen binding energies of all combinations of metals involved in this work. Compositions where a bimetallic material is predicted to be the most active are hatched. Combinations predicted to have surfaces with favorable HER thermodynamics are shown in blue, demonstrating approximately a 50 % reduction in search space across all combinations or a 30 % reduction in combinations where a bimetallic material was expected to form (hatched). Pure aluminum was not predicted to form a metastable metal.

demonstrating that machine learning can be used to aid discovery by finding complex overlapping trends in large datasets. Because they make numerical predictions, such models can give insight into the scope and accuracy of current understanding in a way that qualitative explanations do not, and deviations from fitted models can guide scientists toward areas where new research is most needed. This work considers the ability of a single well-known trend to describe a complex dataset that poses many of the same problems as industrial design; the challenges in proving the presence of a well-established relationship in such a dataset point to the need for additional computational work to describe other physical phenomena in high throughput.

CRediT authorship contribution statement

Kirby Broderick: Ideas; formulation or evolution of overarching research goals and aims, Development or design of methodology; creation of models, Programming; software development; designing computer programs; implementation of the computer code and supporting algorithms; testing of existing code components, Verification, whether as a part of the activity or separate, of the overall replication/reproducibility of results/experiments and other research outputs, Application of statistical, mathematical, computational, or other formal techniques to analyze or synthesize study data, Management activities to annotate (produce metadata), scrub data and maintain research data (including software code, where it is necessary for interpreting the data itself) for initial use and later reuse, Preparation, creation and/or presentation of the published work, specifically writing the initial draft (including substantive translation), Preparation, creation and/or presentation of the published work, specifically visualization/data presentation. **Eric Lopato:** Programming, software development; designing computer programs; implementation of the computer code and supporting algorithms; testing of existing code components, Conducting a research and investigation process, specifically performing the experiments, or data/evidence collection, Preparation, creation and/or presentation of the published work by those from the original research group, specifically critical review, commentary or revision Ű including pre-or postpublication stages. **Brook Wander:** Programming; software development; designing computer programs; implementation of the computer code and supporting algorithms; testing of existing code components. **Stefan Bernhard:** Provision of study materials, reagents, materials, patients, laboratory samples, animals, instrumentation, computing resources, or other analysis tools, Preparation, creation and/or presentation of the published work by those from the original research group, specifically critical review, commentary or revision Ű including pre-or postpublication stages, Management and coordination responsibility for the research activity planning and execution Acquisition of the financial support for the project leading to this publication. **John Kitchin:** Ideas; formulation or evolution of overarching research goals and aims, Preparation, creation and/or presentation of the published work by those from the original research group, specifically critical review, commentary or revision Űincluding pre-or postpublication stages, Oversight and leadership responsibility for the research activity planning and execution, including mentorship external to the core teams, Acquisition of the financial support for the project leading to this publication. **Zachary Ulissi:** Ideas; formulation or evolution of overarching research goals and aims, Provision of study materials, reagents, materials, patients, laboratory samples, animals, instrumentation, computing resources, or other analysis tools, Preparation, creation and/or presentation of the published work by those from the original research group, specifically critical review, commentary or revision Ű including pre-or postpublication stages, Oversight and leadership responsibility for the research activity planning and execution, including mentorship external to the core teams, Management and coordination responsibility for the research activity planning and execution, Acquisition of the financial support for the project leading to this publication.

D. ata and Code Availability

Data used in this work as well as code for generating all figures is available at https://github.com/ulissigroup/DOE_HER.

Declaration of Competing Interest

The authors declare that they have no known competing financial interests or personal relationships that could have appeared to influence the work reported in this paper.

Data Availability

Data and code will be made available freely online.

Acknowledgement

This research was supported by the Department of Energy, Office of Science, Office of Basic Sciences, Data Science for Knowledge Discovery for Chemical and Materials Research Program, under Award DE-SC0020392. The authors thank Kevin Tran for helpful discussions and Adeesh Kolluru for help using Open Catalyst Project resources and optimizing relaxations. E.M.L. was supported by the Steinbrenner Institute Graduate Fellowship and the ARCS Foundation Pittsburgh Chapter.

Appendix A. Detailed experimental methods

A.1. Metal-cation precursors

Metal-cation precursors used included: nickel(II) chloride anhydrous, Alfa Aesar B22085; potassium tetrachloroplatinate(II), Alfa Aesar 11048; ruthenium(III) chloride hydrate, Sigma-Aldrich 206229; molybdenum(III) chloride, Beantown Chemical 132345; potassium tetrachloropalladate(II), Beantown Chemical 129355; lead(II) chloride, Sigma-Aldrich 268690; tin(II) chloride dihydrate, Fisher Scientific S25578; silver trifluoromethanesulfonate, Alfa Aesar, 88722; aluminum trifluoromethanesulfonate, Oakwood Chemical, 003954; gold(III) chloride, Strem Chemical, 93-7907; bismuth(II) chloride, TCI, B3546; cobalt (II) chloride, Alfa Aesar, B22031; chromium(III) chloride hexahydrate, Strem Chemical, 93–2417; europium(III) chloride hexahydrate, Sigma-Aldrich, 203254; iron(II) chloride tetrahydrate, Sigma-Aldrich, 22,029-9; gallium nitrate hydrate, Alfa Aesar, 11150; indium(I) chloride, Alfa Aesar, 40033; iridium(III) chloride hydrate, J&J Materials, 408828; lanthanum(III) chloride, Strem Chemical, 93-5708; lithium chloride, Acros, 199881000; manganese(II) chloride, Beantown Chemical, 137725; osmium(III) chloride hydrate, Acros, 318705000; rhodium (III) chloride hydrate, Thermo-Fischer, 900030512; vanadium(III) chloride, Strem Chemical, 23-4300; and zinc chloride, Alfa Aesar, 87900.

References

[1] U. S. D. of Energy OSTI, Basic research needs for catalysis science, 2017. ⟨https://doi.org/10.2172/1545774⟩, ⟨https://www.osti.gov/biblio/1545774⟩.
[2] K. Tran, Z.W. Ulissi, Active learning across intermetallics to guide discovery of electrocatalysts for CO_2 reduction and H_2 evolution, Nat. Catal. 1 (9) (2018) 696–703.
[3] A.J. Medford, A. Vojvodic, J.S. Hummelshøj, J. Voss, F. Abild-Pedersen, F. Studt, T. Bligaard, A. Nilsson, J.K. Nørskov, From the Sabatier principle to a predictive theory of transition-metal heterogeneous catalysis, J. Catal. 328 (2015) 36–42.
[4] S. Trasatti, Work function, electronegativity, and electrochemical behaviour of metals: III. Electrolytic hydrogen evolution in acid solutions, J. Electroanal. Chem. Interfacial Electrochem. 39 (1) (1972) 163–184.
[5] H. Ooka, J. Huang, K.S. Exner, The Sabatier principle in electrocatalysis: basics, limitations, and extensions, Front. Energy Res. 9 (2021) 155.
[6] J.K. Nørskov, T. Bligaard, A. Logadottir, J. Kitchin, J.G. Chen, S. Pandelov, U. Stimming, Trends in the exchange current for hydrogen evolution, J. Electrochem. Soc. 152 (3) (2005) J23.
[7] J. Greeley, T.F. Jaramillo, J. Bonde, I. Chorkendorff, J.K. Nørskov, Computational high-throughput screening of electrocatalytic materials for hydrogen evolution, Nat. Mater. 5 (11) (2006) 909–913.
[8] E. Skúlason, V. Tripkovic, M.E. Björketun, S. Gudmundsdóttir, G. Karlberg, J. Rossmeisl, T. Bligaard, H. Jónsson, J.K. Nørskov, Modeling the electrochemical hydrogen oxidation and evolution reactions on the basis of density functional theory calculations, J. Phys. Chem. C 114 (42) (2010) 18182–18197.
[9] J. Klicpera, F. Becker, S. Günnemann, Gemnet: universal directional graph neural networks for molecules, arXiv preprint arXiv:2106.08903, 2021.
[10] L. Chanussot, A. Das, S. Goyal, T. Lavril, M. Shuaibi, M. Riviere, K. Tran, J. Heras-Domingo, C. Ho, W. Hu, et al., Open Catalyst 2020 (OC20) dataset and community challenges, ACS Catal. 11 (10) (2021) 6059–6072.
[11] A. Khorshidi, J. Violet, J. Hashemi, A.A. Peterson, How strain can break the scaling relations of catalysis, Nat. Catal. 1 (4) (2018) 263–268.
[12] S. Mitchell, R. Qin, N. Zheng, J. Pérez-Ramírez, Nanoscale engineering of catalytic materials for sustainable technologies, Nat. Nanotechnol. 16 (2) (2021) 129–139.
[13] R. Vallee, M. Wautelet, J. Dauchot, M. Hecq, Size and segregation effects on the phase diagrams of nanoparticles of binary systems, Nanotechnology 12 (1) (2001) 68.
[14] Z. Yang, W. Gao, Applications of machine learning in alloy catalysts: rational selection and future development of descriptors, Adv. Sci. (2022), 2106043.
[15] N. Toshima, T. Yonezawa, Bimetallic nanoparticles-novel materials for chemical and physical applications, New J. Chem. 22 (11) (1998) 1179–1201.
[16] A.K. Singh, Q. Xu, Synergistic catalysis over bimetallic alloy nanoparticles, ChemCatChem 5 (3) (2013) 652–676.
[17] J.K. Nørskov, J. Rossmeisl, A. Logadottir, L. Lindqvist, J.R. Kitchin, T. Bligaard, H. Jonsson, Origin of the overpotential for oxygen reduction at a fuel-cell cathode, J. Phys. Chem. B 108 (46) (2004) 17886–17892.
[18] J. Zheng, J. Nash, B. Xu, Y. Yan, Perspective-towards establishing apparent hydrogen binding energy as the descriptor for hydrogen oxidation/evolution reactions, J. Electrochem. Soc. 165 (2) (2018) H27.
[19] E. Santos, P. Quaino, W. Schmickler, Theory of electrocatalysis: hydrogen evolution and more, Phys. Chem. Chem. Phys. 14 (32) (2012) 11224–11233.
[20] N. Dubouis, A. Grimaud, The hydrogen evolution reaction: from material to interfacial descriptors, Chem. Sci. 10 (40) (2019) 9165–9181.
[21] W. Liu, J. Benson, C. Dawson, A. Strudwick, A.P.A. Raju, Y. Han, M. Li, P. Papakonstantinou, The effects of exfoliation, organic solvents and anodic activation on the catalytic hydrogen evolution reaction of tungsten disulfide, Nanoscale 9 (36) (2017) 13515–13526.
[22] Q. Nian, X. Zhang, Y. Feng, S. Liu, T. Sun, S. Zheng, X. Ren, Z. Tao, D. Zhang, J. Chen, Designing electrolyte structure to suppress hydrogen evolution reaction in aqueous batteries, ACS Energy Lett. 6 (6) (2021) 2174–2180.
[23] E.M. Lopato, E.A. Eikey, Z.C. Simon, S. Back, K. Tran, J. Lewis, J.F. Kowalewski, S. Yazdi, J.R. Kitchin, Z.W. Ulissi, et al., Parallelized screening of characterized and DFT-modeled bimetallic colloidal cocatalysts for photocatalytic hydrogen evolution, ACS Catal. 10 (7) (2020) 4244–4252.
[24] M. Bhat, E.M. Lopato, Z.C. Simon, J.E. Millstone, S. Bernhard, J.R. Kitchin, Accelerated optimization of pure metal and ligand compositions for light-driven hydrogen production, React. Chem. Eng. (2022).
[25] Z.C. Simon, E.M. Lopato, M. Bhat, P.J. Moncure, S.M. Bernhard, J.R. Kitchin, S. Bernhard, J.E. Millstone, Ligand enhanced activity of in situ formed nanoparticles for photocatalytic hydrogen evolution, ChemCatChem 14 (2) (2022), e202101551.
[26] R. Pokhrel, M.K. Goetz, S.E. Shaner, X. Wu, S.S. Stahl, The "best catalyst" for water oxidation depends on the oxidation method employed: a case study of manganese oxides, J. Am. Chem. Soc. 137 (26) (2015) 8384–8387.
[27] S.P. Ong, W.D. Richards, A. Jain, G. Hautier, M. Kocher, S. Cholia, D. Gunter, V. L. Chevrier, K.A. Persson, G. Ceder, Python materials genomics (pymatgen): a robust, open-source python library for materials analysis, Comput. Mater. Sci. 68 (2013) 314–319.
[28] J.R. Boes, O. Mamun, K. Winther, T. Bligaard, Graph theory approach to high-throughput surface adsorption structure generation, J. Phys. Chem. A 123 (11) (2019) 2281–2285.
[29] A.K. Singh, L. Zhou, A. Shinde, S.K. Suram, J.H. Montoya, D. Winston, J. M. Gregoire, K.A. Persson, Electrochemical stability of metastable materials, Chem. Mater. 29 (23) (2017) 10159–10167.
[30] K.A. Persson, B. Waldwick, P. Lazic, G. Ceder, Prediction of solid-aqueous equilibria: scheme to combine first-principles calculations of solids with experimental aqueous states, Phys. Rev. B 85 (23) (2012), 235438.
[31] A.M. Patel, J.K. Nørskov, K.A. Persson, J.H. Montoya, Efficient Pourbaix diagrams of many-element compounds, Phys. Chem. Chem. Phys. 21 (45) (2019) 25323–25327.
[32] M.S. Lowry, J.I. Goldsmith, J.D. Slinker, R. Rohl, R.A. Pascal, G.G. Malliaras, S. Bernhard, Single-layer electroluminescent devices and photoinduced hydrogen production from an ionic iridium (III) complex, Chem. Mater. 17 (23) (2005) 5712–5719.
[33] M. Chen, Y. Han, T.W. Goh, R. Sun, R.V. Maligal-Ganesh, Y. Pei, C.-K. Tsung, J. W. Evans, W. Huang, Kinetics, energetics, and size dependence of the transformation from Pt to ordered PtSn intermetallic nanoparticles, Nanoscale 11 (12) (2019) 5336–5345.
[34] T. Ma, S. Wang, M. Chen, R.V. Maligal-Ganesh, L.-L. Wang, D.D. Johnson, M. J. Kramer, W. Huang, L. Zhou, Toward phase and catalysis control: tracking the formation of intermetallic nanoparticles at atomic scale, Chem 5 (5) (2019) 1235–1247.

[35] J.T. Gamler, A. Leonardi, H.M. Ashberry, N.N. Daanen, Y. Losovyj, R.R. Unocic, M. Engel, S.E. Skrabalak, Achieving highly durable random alloy nanocatalysts through intermetallic cores, ACS Nano 13 (4) (2019) 4008–4017.
[36] C.B. Wahl, M. Aykol, J.H. Swisher, J.H. Montoya, S.K. Suram, C.A. Mirkin, Machine learning-accelerated design and synthesis of polyelemental heterostructures, Sci. Adv. 7 (52) (2021), eabj5505.
[37] J. Li, S. Sun, Intermetallic nanoparticles: synthetic control and their enhanced electrocatalysis, Acc. Chem. Res. 52 (7) (2019) 2015–2025.
[38] A. Palizhati, W. Zhong, K. Tran, S. Back, Z.W. Ulissi, Toward predicting intermetallics surface properties with high-throughput dft and convolutional neural networks, J. Chem. Inf. Model. 59 (11) (2019) 4742–4749.
[39] P. Quaino, F. Juarez, E. Santos, W. Schmickler, Volcano plots in hydrogen electrocatalysis-uses and abuses, Beilstein J. Nanotechnol. 5 (1) (2014) 846–854.
[40] P. Rheinländer, S. Henning, J. Herranz, H.A. Gasteiger, Comparing hydrogen oxidation and evolution reaction kinetics on polycrystalline platinum in 0.1 m and 1 m KOH, ECS Trans. 50 (2) (2013) 2163.
[41] K. Frey, D.J. Schmidt, C. Wolverton, W.F. Schneider, Implications of coverage-dependent O adsorption for catalytic NO oxidation on the late transition metals, Catal. Sci. Technol. 4 (12) (2014) 4356–4365.
[42] A.C. Lausche, A.J. Medford, T.S. Khan, Y. Xu, T. Bligaard, F. Abild-Pedersen, J. K. Nørskov, F. Studt, On the effect of coverage-dependent adsorbate-adsorbate interactions for CO methanation on transition metal surfaces, J. Catal. 307 (2013) 275–282.
[43] P. Lindgren, G. Kastlunger, A.A. Peterson, A challenge to the $\Delta G \sim 0$ interpretation of hydrogen evolution, ACS Catal. 10 (1) (2019) 121–128.
[44] H. Ooka, M.E. Wintzer, R. Nakamura, Non-zero binding enhances kinetics of catalysis: machine learning analysis on the experimental hydrogen binding energy of platinum, ACS Catal. 11 (10) (2021) 6298–6303.
[45] Z. Ulissi, V. Prasad, D. Vlachos, Effect of multiscale model uncertainty on identification of optimal catalyst properties, J. Catal. 281 (2) (2011) 339–344.
[46] D.E. Schipper, Z. Zhao, H. Thirumalai, A.P. Leitner, S.L. Donaldson, A. Kumar, F. Qin, Z. Wang, L.C. Grabow, J. Bao, et al., Effects of catalyst phase on the hydrogen evolution reaction of water splitting: preparation of phase-pure films of FeP, Fe_2P, and Fe_3P and their relative catalytic activities, Chem. Mater. 30 (10) (2018) 3588–3598.
[47] T.D. Tran, M.T. Nguyen, H.V. Le, D.N. Nguyen, Q.D. Truong, P.D. Tran, Gold nanoparticles as an outstanding catalyst for the hydrogen evolution reaction, Chem. Commun. 54 (27) (2018) 3363–3366.
[48] F.W. Campbell, S.R. Belding, R. Baron, L. Xiao, R.G. Compton, The hydrogen evolution reaction at a silver nanoparticle array and a silver macroelectrode compared: changed electrode kinetics between the macro-and nanoscales, J. Phys. Chem. C 113 (33) (2009) 14852–14857.
[49] M.A. Amin, S.A. Fadlallah, G.S. Alosaimi, In situ aqueous synthesis of silver nanoparticles supported on titanium as active electrocatalyst for the hydrogen evolution reaction, Int. J. Hydrog. Energy 39 (34) (2014) 19519–19540.
[50] G. Merga, N. Saucedo, L.C. Cass, J. Puthussery, D. Meisel, "Naked" gold nanoparticles: synthesis, characterization, catalytic hydrogen evolution, and SERS, J. Phys. Chem. C 114 (35) (2010) 14811–14818.
[51] H. Falsig, B. Hvolbæk, I.S. Kristensen, T. Jiang, T. Bligaard, C.H. Christensen, J. K. Nørskov, Trends in the catalytic CO oxidation activity of nanoparticles, Angew. Chem. 120 (26) (2008) 4913–4917.